Available online at www.sciencedirect.com
SCIENCE DIRECT®
Environmental Modelling & Software 19 (2004) 113–128
Environmental Modelling & Software
www.elsevier.com/locate/envsoft

Long-term simulation of global dust distribution with the GOCART model: correlation with North Atlantic Oscillation

P. Ginoux [a,b,*], J.M. Prospero [c], O. Torres [b,d], M. Chin [b]

[a] GEST, University of Maryland Baltimore County, Baltimore, MD, USA
[b] NASA GSFC, Code 916, Greenbelt, MD, USA
[c] RSMAS, University of Miami, FL, USA
[d] JCET, University of Maryland Baltimore County, Baltimore, MD, USA

Received 16 January 2003; received in revised form 4 February 2003; accepted 18 February 2003

Abstract

Global distribution of aeolian dust is simulated from 1981 to 1996 with the Global Ozone Chemistry Aerosol Radiation and Transport (GOCART) model. The results are compared with in situ measurements and satellite data. An index is calculated from the model results and the satellite viewing angles to allow quantitative comparison with the Total ozone mapping spectrometer (TOMS) absorbing aerosol index. The annual budget over the different continents and oceans are analyzed. The simulated annual emission varies from a minimum of 1950 Tg in 1996 to a maximum of 2400 Tg in 1988. Of these emissions, 65% is from North Africa and 25% from Asia. It is found that North America received twice as much dust from other continents than it emits per year. There is no significant trend over the 16-year simulation. The inter-annual variability of dust distribution is analyzed over the North Atlantic and Africa. It is found that in winter a large fraction of the North Atlantic and Africa dust loading is correlated with the North Atlantic Oscillation (NAO) index. It is shown that a controlling factor of such correlation can be attributed to dust emission from the Sahel. The Bodele depression is the major dust source in winter and its inter-annual variability is highly correlated with the NAO. However, the long record of dust concentration measured at Barbados indicates that there is no correlation with the NAO index and surface concentration in winter. Longer simulation should provide the information needed to understand if the effects of the NAO on dust distribution is rather limited or Barbados is at the edge of the affected region.

Keywords: Atmospheric modeling; Dust; North Atlantic Oscillation

1. Introduction

Mineral dust has an impact on the different components of the Earth system. Several studies have shown that dust particles, by absorbing and scattering solar radiation, modify the atmospheric radiative budget (e.g. Tegen and Lacis, 1996; Sokolik and Toon, 1996; Weaver et al., 2002). Dust could also play a positive role in reducing global warming by greenhouse gas CO_2. Carbon fixation by phytoplankton in the oceans acts as a sink for CO_2. Aeolian dust deposition is the primary source of bio-available iron in the iron-limited open oceans and effectively controls phytoplankton blooming (Martin and Gordon, 1988). Another important effect of dust particles is their role in the photochemical production of tropospheric ozone by reducing by as much as 50% the photolysis rates (e.g. Dickerson et al., 1997; Liao et al., 1999; Martin et al., 2002) and by providing reaction sites for ozone and nitrogen molecules (e.g. Prospero et al., 1995; Dentener et al., 1996). Finally, dust particles affect air quality (Prospero, 1999) and are potential vectors for long range transport of bacteria (Prospero et al., in press).

In situ measurements since the 1960s have shown strong daily, seasonal and inter-annual variations of dust concentration over the Atlantic (Prospero, 1999). Aerosol satellite data have been helpful to locate the major dust sources (Herman et al., 1997; Prospero et al., 2002) and to study the variability of aerosol distributions with

* Corresponding author. Address: NOAA GFDL, Forrestal Campus, Route 1, 08542-0308 Princeton NJ, USA. Tel.: +1-609-987-5071; fax: +1-609-987-5063.
E-mail address: paul.ginoux@noaa.gov (P. Ginoux).

1364-8152/$ - see front matter © 2003 Elsevier Ltd. All rights reserved.
doi:10.1016/S1364-8152(03)00114-2

data from the late 1970s (Herman et al., 1997; Torres et al., 2002). It is thus important to better understand the long-term variability of dust distribution, in particular to determine which processes are controlling such variability. Hurrell (1995) has shown that the circulation and precipitation over Europe and the North Atlantic is modulated by the North Atlantic Oscillation (NAO) with a period of about 8 years. Moulin et al. (1997) suggested that the dust distribution over the Atlantic was correlated with the NAO, using satellite data and the long-term measurement of dust concentration at Barbados. More recently, Chiapello and Moulin (2002) showed that in winter there is a significant influence of the NAO on the year-to-year variability of dust export from Africa, as seen from total ozone mapping spectrometer (TOMS) and Meteosat satellite data. Transport models solve explicitly the emission, transport and removal processes. Therefore, they can provide more detailed information on the major processes controlling the spatial and temporal variability of dust distribution. Mahowald et al. (2002) have used a tri-dimensional transport model to understand the 30-year Barbados dust record. Their analysis suggested that the Barbados dust variability could be in part related by disturbed soils in Africa. But they recognized that their analysis is severely limited by the accuracy of the available meteorological data sets. Ginoux et al. (2001) have developed a transport dust model whose emission is solely based on natural sources. Over a 5-year simulation, it seemed that such sources are sufficient to reproduce reasonably well most characteristics of dust distribution at the global scale. In this paper, the simulation is extended and covers 16 years from 1981 to 1996. The results of this simulation are used to analyze the year-to-year variation of dust distribution with a focus on North Africa and the Atlantic. After describing briefly the transport model used to simulate dust distribution, the budget over the continents and oceans will be discussed before comparing the model results with in situ and satellite data. Finally, the effects of the NAO on dust emission, concentration and mass column will be analyzed.

2. Model description

The model used for this study is the Global Ozone Chemistry Aerosol Radiation and Transport (GOCART) model. The GOCART model simulates the distribution of dust, sulfate, carbonaceous (organic and black carbon), and sea-salt aerosols. Each model component has been described in detail elsewhere (Chin et al., 2000; Ginoux et al., 2001; Chin et al., 2002), and their combined effect on total optical thickness has been compared with in situ measurements and satellite retrievals (Chin et al., 2002). Briefly, the GOCART model is a global scale model driven by the Goddard Earth Observing System Data Assimilation System (GEOS DAS). It has a horizontal resolution of 2° latitude by 2.5° longitude and 20–40 vertical layers (vertical resolution depends on the version of GEOS DAS). The model contains the following modules in aerosol simulation: emission, which includes dust, sulfur, black carbon, organic carbon, and sea-salt emissions; chemistry, which includes in-air and in-cloud oxidations of sulfate precursors (SO_2 and DMS); advection, which is computed by a flux-form semi-Lagrangian method; boundary layer turbulent mixing, which uses a second order closure scheme; moist convection, which is calculated using archived cloud mass flux fields; dry deposition at the surface by eddies; wet deposition, which accounts for the scavenging of soluble species in convective updrafts and rainout/washout in large-scale precipitation.

More detailed description and references are given in Chin et al. (2000) for sulfate, Ginoux et al. (2001) for dust, and Chin et al. (2002) for the other aerosols. Dust distribution from GOCART model has been used to derive optical properties from the TOMS data (Torres et al., 2002), to calculate radiative forcing (Weaver et al., 2002), to study the effects of heterogeneous reactions on O_3 photochemistry (Martin et al., 2002), and to study the effects of phytoplankton blooming by dust deposition at the ocean surface with a global ocean circulation–ecosystem model (Gregg et al., in press).

Dust size distribution is calculated by solving the continuity equation for a discrete number of size bins. The size distribution of mineral dust ranges from 0.1 μm for clay to several hundreds micrometer for sand. However, the total volume (or mass) of particles larger than 10 μm is several orders of magnitude lower than for smaller particles, and the maximum of the volume is around 2 μm radius (Dubovik et al., 2002). The occurrence of particles larger than 1 μm is primarily constrained by gravitational settling. In GOCART model, the size distribution is discretized into four size bins: 0.1–1, 1–2, 2–3, and 3–6 μm radius. The physical parameters of these four bins are given in Table 1. The continuity equation includes macroscopic advection by winds, parameterized eddy diffusion and moist convection. The removal mechanisms include dry deposition at the surface by impaction, wet deposition in and below clouds, and gravitational settling. Dust is uplifted by wind over preferential sources, as opposed to any desert area, which have been associated with topographic lows.

2.1. Dust sources

The approach used in GOCART to identify the major dust sources is based on the analysis by Prospero et al. (2002). Using the TOMS aerosol index (TOMS AI) (available at http://toms.gsfc.nasa.gov), they have identified and characterized the geomorphological nature of the major dust sources. Most of these sources correspond

Table 1
Physical properties of the transported size bins

Bin	Radius range (μm)	Size distribution	Source fraction	r_i (μm)	ρ_{pi} (kg/m^3)
1	0.1–1	$dm/d\ln r$ = cst	0.1	0.75	2600
2	1–2	dm/dr = cst	0.25	1.5	2600
3	2–3	dm/dr = cst	0.25	2.5	2600
4	3–6	dm/dr = cst	0.25	4.5	2600

to dry lakes or riverbeds where a sufficiently deep layer of alluvium was able to accumulate. Their analysis also found that human impacts are not as important as previously suggested. Because of the global nature of these findings, the relative altitude of any point in the surrounding basin has been used as a global dust source function. A problem with a continuous function is that any point can emit dust particles. To increase the contrast between the topographic lows and their surrounding, an exponent is added to the function. Laboratory and field measurements (e.g. Marticorena and Bergametti, 1995) have shown the importance of surface roughness for dust uplifting. Vegetation will increase the surface roughness and decrease or prevent dust emission. In the model, the function is calculated only over bare soils retrieved from satellite data. The function is supposed to be invariant in time, although the vegetation cover changes with time. The justification is that it is unclear if the error associated with satellite retrieval of ground cover over active dust sources are low enough to provide reliable vegetation cover. The inclusion of a time dependent vegetation cover in the source function by Mahowald et al. (2002) seems to slightly degrade the correlation between the model predictions and the observations. The dust source function has served for the present and future scenarios of the Intergovernmental Panel for Climate Change (Penner et al., 2001) and model intercomparison (Penner et al., 2002), is used by several global and regional model (e.g. Mahowald et al., 2002; Alpert et al., 2002; Barnum et al., this issue). Fig. 1 shows the global distribution of the source function on one degree grid, and the 10-year average TOMS absorbing aerosol index. In the arid regions, the location of the maxima of the TOMS index and source function seems to correspond. In the tropical regions, the TOMS data indicate the presence of large amount of aerosols but these are particles of black carbon which are associated with biomass burning of savannah or forest (Torres et al., 2002).

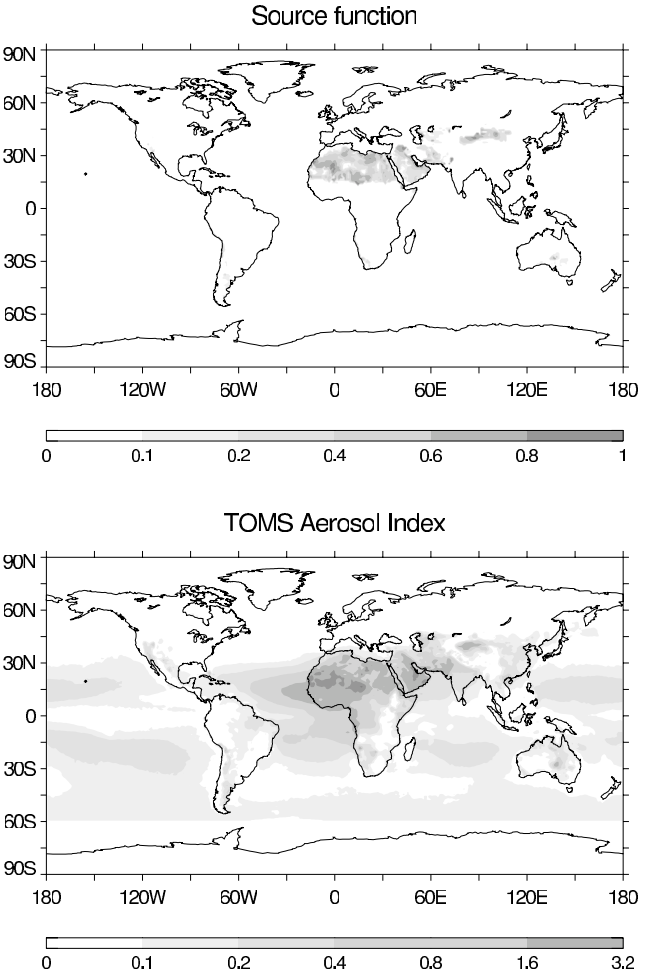

Fig. 1. Global distribution of the dust sources on GOCART grid (upper panel) and of the TOMS absorbing aerosol index average from 1981 to 1990 (lower panel).

2.2. Dust emission

Dust uplift into the atmosphere is mainly initiated by saltation bombardment (sand blasting). In GOCART, the vertical flux of dust particles is assumed to be proportional to the horizontal flux of sand particles, and it is approximated by an expression similar to the empirical formula developed by Gillette and Passi (1988):

$$F_p = \begin{cases} CSs_p u_{10\,\mathrm{m}}^2 (u_{10\,\mathrm{m}} - u_{tp}) & \text{if } u_{10\,\mathrm{m}} > u_t \\ 0 & \text{otherwise} \end{cases}, \quad (1)$$

where C is a dimensional factor equal to 1 μg s^2 m^{-5}, S is the source function described by Ginoux et al. (2001), $u_{10\,\mathrm{m}}$ is the horizontal wind speed at 10 m, u_{tp} is the threshold velocity for class p, and s_p is the fraction of each size classes given in Table 1.

The threshold velocity for wind erosion is calculated

from the Iversen and White (1982) numerical formulation with the simplications proposed by Marticorena and Bergametti (1995). The expression of the threshold velocity for class p, in units of m s^{-1}, is given by

$$u_{tp} = 0.13 \frac{\sqrt{\frac{\rho_p g \Phi_p}{\rho_a}} \sqrt{1 + \frac{6 \times 10^{-7}}{\rho_p g \Phi_p^{2.5}}}}{\sqrt{1.7638(4.6 \times 10^6 [\Phi_p^{1.56} + 1]^{0.092} - 1)}}, \quad (2)$$

where ρ_p is the particle density (kg m^{-3}), g is the gravity (9.81 m s^{-2}), Φ_p is the effective diameter of the class p (m), ρ_a is the air density. The values of ρ_p and Φ_p are given for each four classes p in Table 1. To take into account the bonding effect of soil moisture, expression (2) is modified as in Ginoux et al. (2001),

$$u_{twp} = \begin{cases} u_{tp} \times (1.2 + 0.2 \log_{10} w) & \text{if } w < 0.5 \\ \infty & \text{otherwise} \end{cases}, \quad (3)$$

where w is the soil moisture which varies from near zero value in arid region to one over water, snow or ice.

3. Model results

The dust distribution is simulated from January 1981 to December 1996. The instantaneous dust concentration for each of the particle-size four bins at every model grid point is archived every 6 h.

3.1. Global budget

Fig. 2 shows the global annual budget for 16 years. It includes dust emission and removal by wet and dry deposition. Although the lifetime of dust particles is about 1 week, the annual budget is not equilibrated: the annual deposition by dry and wet deposition is systematically higher than the emission. This is an inherent problem of transport models which cannot conserve mass because of time interpolation. The error is of the order of 1%. Dry deposition contributes to 90% of total dust removal. The ratio between dry and wet removal varies by less than 10% over the 16 years simulation. The maximum difference of annual emission is about 23% with the lowest emission in 1996 (1950 Tg) and the highest in 1988 (2400 Tg).

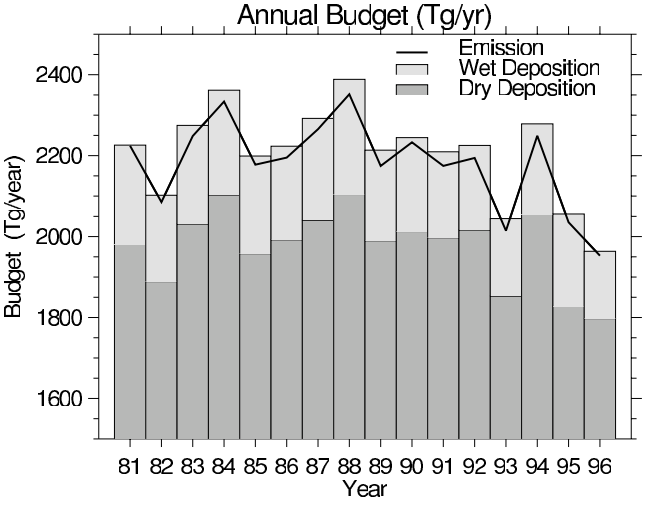

Fig. 2. Global annual budget of dust from 1981 to 1996: emission (line), dry deposition (dark gray boxes), and wet deposition (light gray boxes), in units of Tg year^{-1}.

Table 2 gives the budget over five different regions: North Africa, South Africa, North America, South America and Asia. The annual emission from North Africa is around 1400 Tg year^{-1} which represents 65% of the global emission, while Asia contributes for 25%. The contribution from the other regions is relatively low and of the order of the standard deviation of dust emission from North Africa. Over the 16 years simulation, there is a downward trend of dust emission from Africa and Asia of 6 and 2 Tg year^{-1}, respectively. These values are ten times lower than the standard deviation of the annual emissions. Furthermore, the inter-annual variability of dust emission is relatively low with a maximum relative difference around 20%. Thus, the emission trends are not significant over the simulated period. This is also true for the deposition which follows the variability of the emission rate. The difference between annual emission and deposition is positive for all continents except for North America. Over that continent the annual deposition is three times higher than the emission. This means that long range transport from other continents is controlling the inter-annual variability of dust loading over North America. Perry et al. (1997) have observed African intrusions over continental US with dust concentration exceeding by an order of magnitude the background values in the so-called “dust-bowl” states of the central USA. The dust distribution over North America is also influenced by Asian dust episodes, mainly in spring. Such episodes have been observed from satellite data and forecasted by the GOCART model, among others, during the ACE-Asia field campaign (available at http://code916.gsfc.nasa.gov/Missions/ACEASIA/). These results indicate the importance of inter-continental transport, but further simulations would be needed to know the relative contribution of each continents.

Table 3 gives the annual dry and wet deposition rates for six oceanic regions. The highest deposition rates are in the North Indian Ocean while in the South Indian Ocean the rates are a factor ten lower. The contribution of wet deposition to total removal is the highest over the North Pacific (50%) and the lowest over the South Atlantic (10%). Such a large difference can be explained by the combined effects of precipitation rate and altitude of the dust plume. In East Asia, the dust storms are generated by passing cold fronts which uplifted dust up to

Table 2
Annual budget of dust emission, dry deposition (settling and turbulent transfer), wet deposition, and burden over six continents in units of Tg year^{-1}

Year	North Africa				South Africa				North America				South America				Asia				Australia			
	Emi	Dry	Wet	Bur	Emi	Dry	Wet	Bur	Emi	Dry	Wet	Bur	Emi	Dry	Wet	Bur	Emi	Dry	Wet	Bur	Emi	Dry	Wet	Bur
1981	1461	1067	81	312	26	20	1	4	9	28	11	−30	49	37	4	9	506	419	28	59	61	44	2	16
1982	1369	1028	62	279	23	18	1	4	10	29	10	−30	48	35	4	9	472	397	25	50	59	43	1	15
1983	1507	1107	64	336	22	17	1	4	8	31	13	−36	56	41	6	9	484	397	30	58	55	40	2	13
1984	1538	1120	66	352	24	19	1	3	10	34	15	−39	53	40	7	7	525	434	29	61	58	42	2	14
1985	1408	1037	67	304	22	17	1	4	10	30	12	−33	51	38	5	8	504	416	27	60	67	46	3	19
1986	1397	1044	59	294	23	17	1	4	9	30	13	−34	55	38	5	12	533	430	31	73	60	44	2	14
1987	1459	1079	69	312	27	21	2	4	9	32	13	−36	56	41	6	9	528	432	26	71	67	46	2	19
1988	1544	1121	76	347	19	17	2	0	11	35	14	−37	61	43	6	12	516	426	36	54	71	49	2	20
1989	1416	1065	60	291	21	17	1	3	10	32	12	−33	57	40	5	12	488	399	27	63	53	39	2	12
1990	1446	1085	50	311	20	16	1	3	10	28	11	−29	61	42	5	14	502	404	40	58	65	45	2	18
1991	1380	1056	51	273	19	16	1	2	9	32	11	−34	56	39	5	12	517	420	33	64	63	45	2	17
1992	1466	1085	54	328	20	16	1	3	8	31	11	−34	49	36	4	9	488	423	24	42	58	43	2	13
1993	1350	1019	52	278	22	17	1	4	7	25	10	−27	65	45	5	15	398	343	22	32	57	41	2	14
1994	1431	1053	49	329	21	18	1	3	9	34	13	−38	58	42	5	11	530	438	33	58	64	44	2	18
1995	1415	1063	68	284	19	17	1	2	7	28	12	−32	56	41	5	11	504	416	27	60	71	48	2	21
1996	1288	971	36	281	24	19	1	4	8	32	11	−36	44	33	4	7	435	355	19	62	52	39	1	12
Mean	1430	1062	60	307	22	17	1	3	9	31	12	−34	55	39	5	10	496	409	29	58	61	44	2	16
Dev	66	38	11	25	2	1	0	1	1	3	1	3	5	3	1	2	35	26	5	10	6	3	0	3
Trend	−6	−3	−2	−2	0	0	0	0	0	0	0	0	0	0	0	0	−2	−2	0	0	0	0	0	0

Table 3
Annual budget of dust dry deposition (settling and turbuelnt transfer) and wet deposition over six oceans in units of Tg year^{-1}

Year	North Atlantic		South Atlantic		North Pacific		South Pacific		North Indian		South Indian	
	Dry	Wet	Dry	Wet	Dry	Wet	Dry	Wet	Dry	Wet	Dry	Wet
1981	117	32	17	2	76	39	20	5	126	37	12	3
1982	101	28	15	2	74	37	20	4	118	36	11	3
1983	148	39	17	3	81	39	20	5	120	38	11	4
1984	135	39	18	3	88	45	22	6	145	42	13	4
1985	119	36	16	3	73	41	23	6	129	36	13	4
1986	129	30	19	2	77	42	22	5	128	38	13	3
1987	124	43	20	3	85	42	25	6	123	35	14	4
1988	130	42	21	4	85	44	27	8	140	47	15	5
1989	137	31	19	3	77	38	21	5	133	38	12	3
1990	133	32	20	2	70	37	24	5	132	44	12	3
1991	117	25	20	2	82	38	24	5	134	38	12	3
1992	144	30	14	2	83	39	20	5	117	35	10	3
1993	130	29	17	2	63	32	22	4	119	30	12	3
1994	144	23	18	3	86	45	24	5	140	40	14	4
1995	124	40	16	2	75	38	23	5	119	36	12	3
1996	112	24	18	1	78	38	22	4	111	25	12	2
Mean	128	33	18	2	78	39	23	5	127	37	12	3
Dev	12	6	2	1	6	3	2	1	9	5	1	1
Trend	0	−1	0	0	0	0	0	0	0	0	0	0

high elevation over Asia (Merrill et al., 1989). Also, these fronts contain precipitating clouds which can remove dust from the atmosphere. In the Western Pacific, the precipitation rates, diagnosed by GEOS DAS, range between 0.5 and 2 m year^{-1} while in the South Atlantic, the rates are as low as 0.1 m year^{-1} in the coastal regions of Namibia (South Africa) and Patagonia (Argentina).

3.2. North-African budget

Table 4 gives the winter, summer and annual budgets over Sahara (North of 21.25° N) and Sahel (South of 21.25° N) in North Africa. The emissions from Sahara are twice the corresponding emissions from Sahel, and represents 64% of North Africa and 42% of global emissions. The standard deviation of dust emissions from Sahel and Sahara are equivalent. This means that there is a stronger inter-annual variability of dust emission over the Sahel. In Sahara, the emissions are 30% higher in summer than in winter, while in Sahel the emissions are slightly higher in winter. In Sahara the wet deposition is negligible compared to the dry deposition, but in Sahel it varies strongly with season: in winter it is negligible but in summer it represents 22% of the removal rate. This can be explained by the movement of the inter-tropical convergence zone (ITCZ) which occupies its northernmost position in summer. The ITCZ is made manifest at the surface by the transition zone between the dry harmattan air and the moist air from the equatorial regions (Mbourou et al., 1997). Table 4 shows that in Sahara, the highest emissions were in 1984 for all seasons, while in Sahel the corresponding year of maximum varies between seasons: 1983 for winter, and 1988 for summer and annual mean. For both regions, the year 1996 has the lowest annual emission. For both regions, there are equivalent downward trends of dust emission.

4. Variability of surface concentration

Fig. 3 shows the global distribution of the mean surface concentration, the seasonal standard deviation, and the annual standard deviation of the 16-year simulation. The figure shows a clear difference of dust loading between the two hemispheres, with a much stronger impact of long range transport in the North hemisphere: dust transported from Africa to the Atlantic and from Asia to the Pacific. The values of seasonal standard deviation are a factor 2 higher than the annual standard deviation, and of the same order of magnitude as the long-term mean, except over the Caribbean, the Taklamakan desert and Indonesia where they are a factor 2–5 higher than the long-term mean. Thus, it seems that the inter-annual variability is of second order compare to the seasonal variation almost everywhere. In few regions (e.g. Strait of Gibraltar) the inter-annual variability is significantly higher. We should note that our relatively short simulation does not cover previous decades with significantly lower surface concentration observed in the Caribbean (Prospero and Nees, 1986) and the year-to-year variability is underestimated.

Table 4
Winter (January–March), summer (June–August) and annual budget of dust emission, dry deposition (settling and turbuelnt transfer), wet deposition, and burden over Sahara (latitude $> 21.25°$ N) and Sahel (latitude $< 21.25°$ N)

Year	Sahara												Sahel											
	Jan–Feb–Mar (Tg 3 month^{-1})				Jun–Jul–Aug (Tg 3 month^{-1})				Annual Tg year^{-1}				Jan–Feb–Mar (Tg 3 month^{-1})				Jun–Jul–Aug (Tg 3 month^{-1})				Annual (Tg year^{-1})			
	Emi	Dry	Wet	Bur	Emi	Dry	Wet	Bur	Emi	Dry	Wet	Bur	Emi	Dry	Wet	Bur	Emi	Dry	Wet	Bur	Emi	Dry	Wet	Bur
1981	215	138	1	76	301	176	4	121	940	602	9	328	158	141	2	14	122	107	40	−25	520	465	72	−16
1982	187	132	1	53	287	169	4	114	875	591	10	275	150	125	2	23	125	112	32	−18	493	438	52	4
1983	219	143	1	75	298	173	3	121	934	602	7	324	184	161	1	22	134	120	35	−21	574	505	57	12
1984	229	149	1	80	319	180	3	136	987	629	8	349	165	152	3	10	152	127	35	−11	551	491	58	2
1985	200	139	0	61	274	158	3	114	878	573	8	297	147	130	2	15	133	113	35	−15	530	464	59	7
1986	200	136	0	64	275	161	3	111	885	574	7	304	141	131	3	7	138	117	31	−10	512	470	52	−10
1987	202	137	1	64	279	167	4	108	895	595	8	292	140	129	2	9	137	118	36	−16	564	483	61	20
1988	226	153	0	73	313	179	4	130	957	624	9	324	174	150	3	22	163	128	43	−8	587	497	67	22
1989	230	152	0	77	262	158	3	102	875	585	6	285	182	157	2	24	128	118	34	−23	541	480	54	6
1990	204	143	0	60	265	158	1	106	881	594	4	283	179	154	2	23	134	116	27	−10	565	491	46	28
1991	196	141	1	55	265	162	2	101	876	601	6	269	143	129	1	13	140	120	29	−10	504	454	45	4
1992	195	143	0	52	278	166	3	110	908	603	7	299	167	142	1	23	141	122	32	−12	558	482	47	29
1993	177	129	1	47	269	160	2	106	831	568	7	256	163	135	2	26	126	111	27	−13	519	451	45	22
1994	224	149	0	75	280	163	2	116	902	584	6	312	162	145	2	15	134	112	26	−4	528	468	43	17
1995	190	127	1	62	290	169	3	118	869	565	8	296	159	143	1	14	136	117	38	−19	509	456	59	−7
1996	177	126	0	51	279	170	1	107	854	570	2	281	117	106	1	9	111	102	22	−12	435	401	34	0
Mean	204	140	1	64	283	167	3	114	897	591	7	298	158	139	2	17	135	116	33	−14	531	468	53	9
Dev	17	8	0	10	16	7	1	9	39	18	2	24	17	14	1	6	11	7	5	6	36	25	9	13
Trend	−1	0	0	−1	−2	−1	0	−1	−5	−2	0	−2	−1	−1	0	0	0	0	−1	1	−3	−2	−1	1

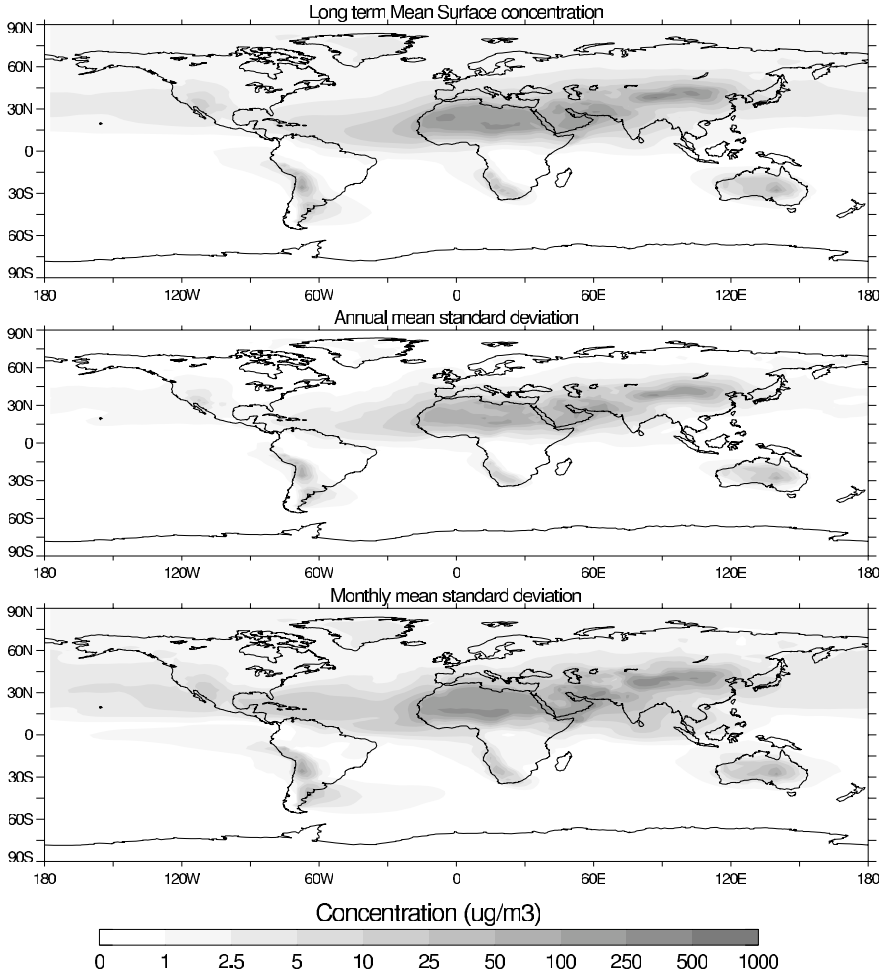

Fig. 3. Long-term dust concentration at the surface (upper panel), standard deviation of the annual concentration (middle panel), and standard deviation of the monthly concentration (lower panel), over 16 years, in units of μg m^{-3}.

4.1. Seasonal variation

Dust samples have been collected in the University of Miami network over the past two decades. The sampling is performed by using high-volume air-sampling systems and Whatman 41 filters to collect dust particles (Savoie and Prospero, 1977). Most sites are located on islands or along the windward coast. Fig. 4 shows the comparison between the observed and simulated monthly concentration at 12 sites. The sites are within the boundary layer (below 100 m), except for Izana which is located at 2360 m above sea-level. The name, coordinates, first and last days of measurements of dust concentration are given in Table 5. The simulated values are averaged over 16 years. The results are very similar to the results presented by Ginoux et al. (2001), although they have used a different parameterization of u_t. As before, the model is performing correctly in the dusty regions but overestimates dust concentrations in the remote regions of the Northern hemisphere: over the Atlantic at Mace Head and over the Pacific at Midway. In the Southern hemisphere, the model results are within the standard deviation of the measurements. Ginoux et al. (2001) suggested that the discrepancy in the remote regions could be due to the parameterization of u_t, but this new simulation indicates that it has another origin. Preliminary results from an improved database of bare surface over China seem to indicate that the model is overestimating dust emission from the loess plateau. Although the source function is quite low over the loess plateau, its high altitude (~3 km above sea-level) is particularly efficient for the long range transport of dust all year long and could explain the model overestimated concentration in the remote regions.

4.2. Inter-annual variation

Fig. 5 shows the comparison between the measured and calculated dust concentrations at Izana, Barbados, Miami, and Bermuda. The data have been collected during the multidisciplinary Atmosphere/Ocean Chemistry Experiment (AEROCE) program (Arimoto et al., 1995, 1999; Prospero, 1999). The correlations coefficient (R) between simulated and observed concentrations is 0.69

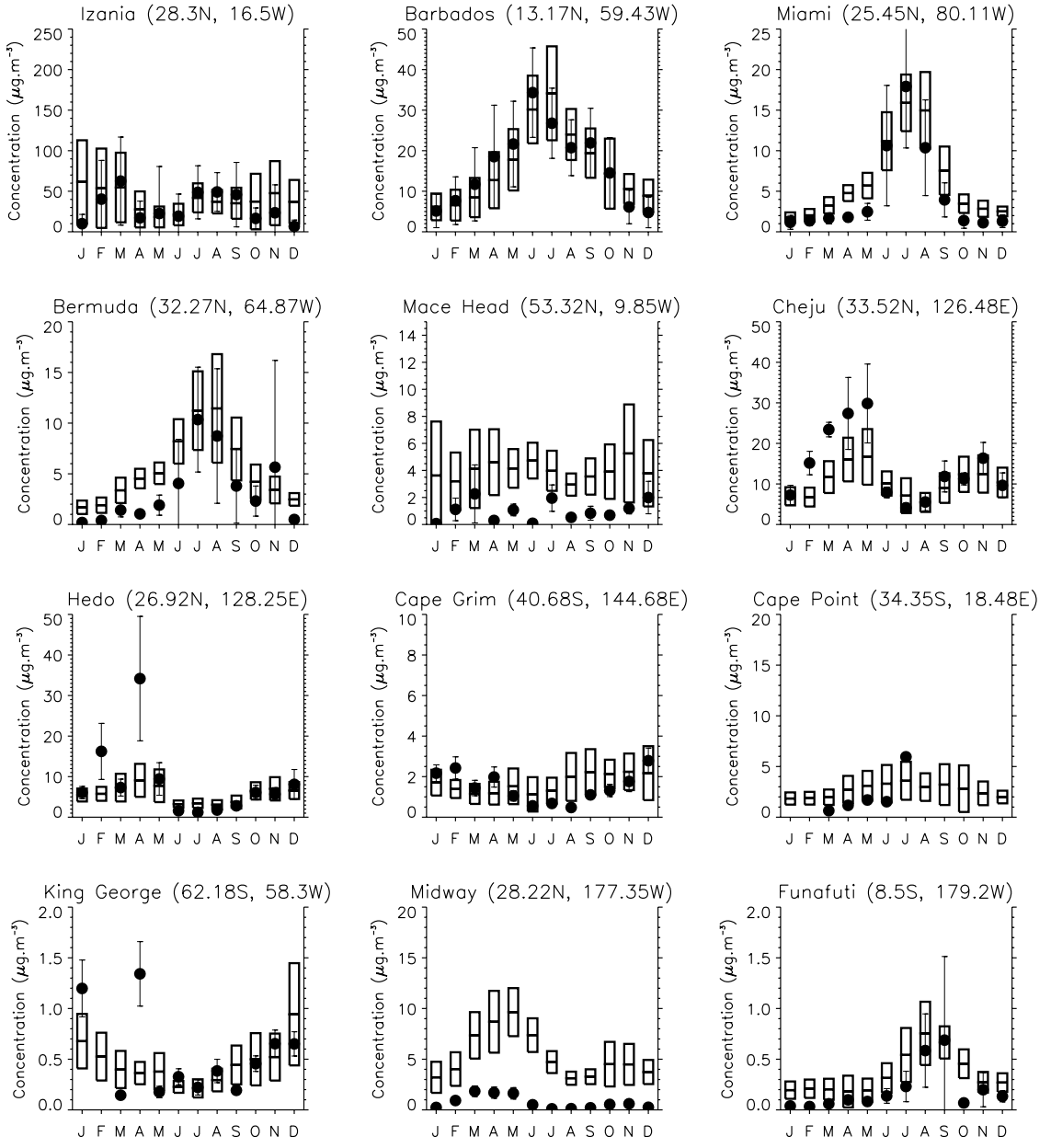

Fig. 4. Comparison of the climatological monthly surface dust concentration, simulated (boxes) and observed (dots) at 12 sites in units of μg m^{-3}, with their standard deviation.

for Izana, 0.79 for Barbados and Miami, and 0.58 for Bermuda. At all stations, the model tends to slightly overestimate dust concentration in winter. The observed seasonal gradient seems to amplify as the distance from African sources increases but the model shows the opposite. The damping of the seasonal variation by the model at Bermuda is quite obvious. It is unclear if this is purely a problem of deposition rate or the combination of different processes. As we will show in the case study of the evolution of a dust plume reaching Bermuda in March 1988, the model has difficulties maintain high concentrations of narrow dust plumes. The model resolution and time interpolation of the meteorological fields tends to increase the numerical diffusion and the background dust concentration while damping the peak values. Such a problem should not affect sites located along the Sahara air layer (SAL) over the Atlantic like Izana or Barbados because the SAL latitudinal width ranges from 10° to 20° (5–10 grid points).

5. TOMS aerosol index

The TOMS instrument on board the satellite Nimbus 7 measured aerosol backscattering radiances at 340 and 380 nm from November 1978 until May 1993. In this

Table 5
List of sites of the University of Miami with their name latitude, longitude, first and last days of measured dust concentration used in Fig. 4

	Name	Latitude	Longitude	First day	Last day
1	Izana	28.3° N	16.5° W	25 Jul 1987	1 Jul 1998
2	Barbados	13.17° N	59.43° W	5 May 1984	1 Jul 1998
3	Miami	25.75° N	80.25° W	2 Jan 1989	7 Aug 1998
4	Bermuda	32.27° N	64.87° W	29 Mar 1989	1 Jan 1998
5	Mace Head	53.32° N	9.85° W	11 Aug 1988	15 Aug 1994
6	Cheju	33.52° N	126.48° E	10 Sep 1991	27 Oct 1995
7	Hedo	26.92° N	128.25° E	1 Sep 1991	18 Mar 1994
8	Cape Grim	40.68° S	144.68° E	11 Jan 1983	8 Nov 1996
9	Cape Point	34.35° S	18.48° E	27 Feb 1992	21 Nov 1996
10	King George	62.18° S	58.3° W	27 Mar 1990	25 Sep 1996
11	Midway	28.22° N	177.35° W	18 Jan 1981	2 Jan 1997
12	Funafuti	8.5° S	179.2° W	8 Apr 1983	31 Jul 1987

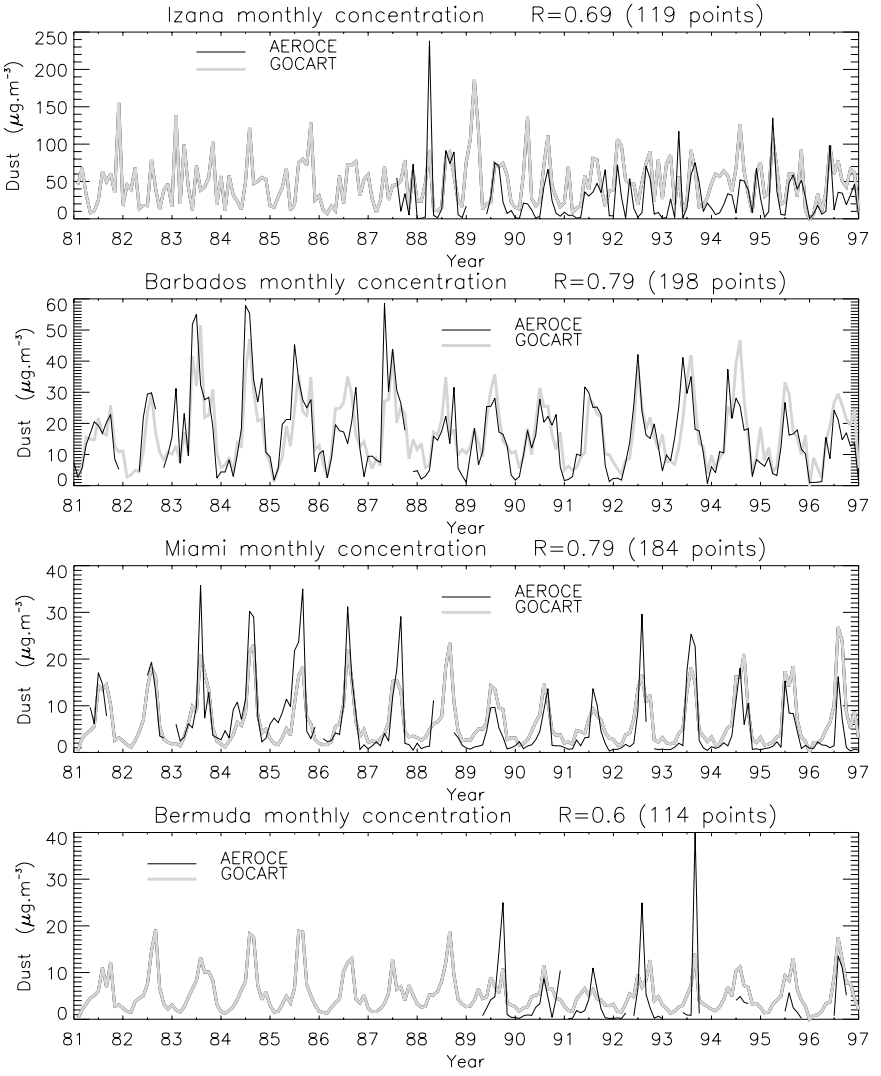

Fig. 5. Monthly dust concentration from January 1981 to December 1996, simulated (gray line) and observed (black line) at Izana (upper panel), Barbados (upper middle panel), Miami (lower middle panel), and Bermuda (lower panel) in units of μg m^{-3}.

study, we use the data from the period 1981–1990. These measurements cover the Earth daily with a 50 km resolution at satellite footprint. The local passing time is about 11:30 a.m. By taking the difference between the measured and calculated radiances for a purely molecular atmosphere, Herman et al. (1997) defined the TOMS AI as follows

$$\mathrm{AI} = -100\left\{\log_{10}\left(\frac{I^{\mathrm{m}}_{340}}{I^{\mathrm{m}}_{380}}\right)-\log_{10}\left(\frac{I^{\mathrm{c}}_{340}}{I^{\mathrm{c}}_{380}}\right)\right\}, \tag{4}$$

where I^{m} is the backscattered radiance measured by TOMS at the given wavelength and I^{c} is the radiance calculated using a radiative transfer model for a pure Rayleigh atmosphere. The TOMS AI is a qualitative indicator of the presence of ultra-violet (UV) absorbing aerosols. An inversion procedure that retrieves aerosol properties from the TOMS radiances has been developed by Torres et al. (1998). They have shown that for UV absorbing aerosols, like dust particles, the optical thickness can be derived from the TOMS AI knowing the values of single scattering albedo, the altitude of the aerosol layer, and the surface pressure. However, the assumed absorption properties in their calculations are an order of magnitude higher than recent investigations (e.g. Colarco et al., 2002). Instead of comparing optical thicknesses retrieved from TOMS and calculated from our model results using different assumptions of optical properties, it is suggested to compare the TOMS AI, for which there is no assumption, and an equivalent index calculated from the model results. Such methodology allows a better control of eventual discrepancies because errors can only be associated with the model results. The equivalent aerosol index is calculated from the satellite viewing angles and the simulated size distribution. The methodology consists to first calculate the optical thickness at 380 nm from the relation:

$$\tau_{380} = \sum_{k=1}^{7} \tau_k = \sum_{k=1}^{7} \frac{3}{4}\frac{Q_k \alpha_k M_i}{r_k \rho_{pi}} \qquad i = 1 \text{ for } k \leq 4 \text{ and } i = k-3 \text{ for } k > 4 \tag{5}$$

where τ_k is the optical thickness at 380 nm for seven bins k, Q_k is the extinction efficiency at 380 nm, M_i is the column mass loading of bin i of the four transported size bins, α_k is the fraction of each seven sub-bins, r_k is the effective radius, and ρ_{pi} is the mass density of the size class i. The values of Q_k (380 nm) are calculated using Mie theory and using the real and imaginary parts of the refractive index derived by Colarco et al. (2002). Second, the single scattering albedo at 380 nm (ω_{380}) is calculated by the relation.

$$\omega_{380} = \frac{\sum_{k=1}^{7} \omega_k \tau_k}{\tau_{380}} \tag{6}$$

where ω_k is the single scattering albedo of particle radius r_k and is calculated using Mie theory and the same values of the refractive index as Q_k. The values of r_k, α_k, Q_k, and ω_k are given in Table 6, and the values of ρ_{pi} are given in Table 1. Third, the centroid of mass Z is calculated by the formula

$$Z = \frac{\sum_{j=1}^{nlev}\left(\sum_{i=1}^{4} m_{i,j}\right) z_j}{\sum_{i=1}^{4} M_i} \tag{7}$$

where z_j is the altitude above ground at level j among the $nlev$ model levels, $m_{i,j}$ is the mass concentration of size class i at level j, and M_i is the mass column. With τ_{380}, ω_{380}, Z, and the TOMS instrument viewing angles, an aerosol index is calculated using the method developed by Torres et al. (1998). Such calculated aerosol index can be directly compared to TOMS index, and is mainly sensitive to the optical thickness and vertical distribution and to a lesser extend to the single scattering albedo (Ginoux and Torres, in press).

Fig. 6 shows the comparison between the observed and calculated aerosol index during a dust storm from Sahara in March 1988. Around 27 March 1988, a dust plume was produced from Sahara and transported by the Azores high towards Europe. Two days later, the plume separated into two branches: one went West and the other East. The West branch formed a half circle two days later over most of the North Atlantic. The model is able to reproduce the evolution of the complex pattern of this intense dust plume. However, the model is unable to maintain the narrow aspect of the plume on the 31st. The simulated widening of the plume is accompanied by a drop of the index by a factor 2. It necessitates a minimum of three grid points to reproduce a spatial gradient, or 6° in latitude and 7.5° in longitude. This dust plume is particularly narrow, less than 5°, and exemplifies the problem of model diffusion and conservation of steep gradients.

The aerosol index has been calculated for a 10-year

Table 6
Optical properties of dust particles used to calculate an aerosol index: effective radius (r_k) of the sub-bin k of the four transported bins (i), size fraction of the sub-bin (α_k), extinction efficiency at 380 nm (Q_k), and single scattering albedo at 380 nm (ω_k)

k	r_k (μm)	i	α_k	Q_k (380 nm)	ω_k (380 nm)
1	0.14	1	0.01	0.732	0.962
2	0.24	1	0.08	0.276	0.976
3	0.45	1	0.25	3.975	0.968
4	0.8	1	0.65	2.427	0.905
5	1.5	2	1	2.354	0.861
6	2.5	3	1	2.228	0.798
7	4.5	4	1	2.182	0.725

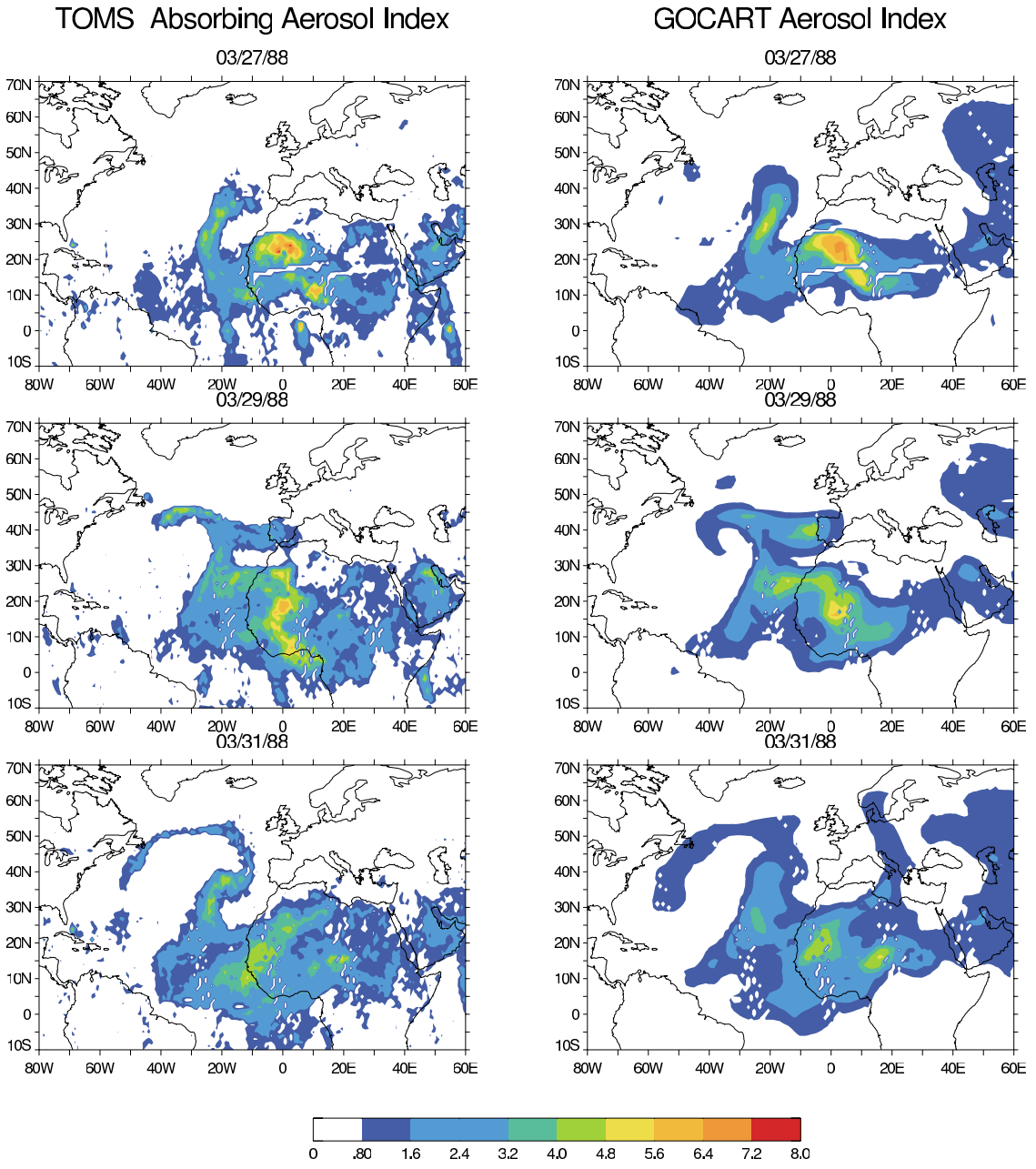

Fig. 6. Comparison between the TOMS absorbing aerosol index (left panels) and simulated index (right panels) during the evolution of a dust plume over the North Atlantic in March 1988.

simulation from January 1981 to December 1990, excluding July 1990 because of problems with TOMS calibration. Fig. 7 shows the global distribution of the correlation coefficient between the observed and simulated aerosol index. Over the arid regions the correlation coefficient is higher than 0.8, as well as over the North Atlantic. Over the North Pacific there is a 15° band with significant correlation but most Asian dust plumes are moving eastward at higher latitudes. It is important to understand that the TOMS AI is sensitive to all absorbing aerosols including dust and black carbon, while the simulated aerosol index considers only dust particles. So, if the seasonal and inter-annual cycle of the simulated dust distribution is in phase with other absorbing aerosols there will be a positive correlation. Such phase correlation is apparent in the biomass burning regions over South America where smoke aerosols are emitted. This could also be true over the North Pacific. When comparing surface dust concentrations at Midway, we showed that the simulated values are overestimated. If the model overestimates dust loading in the remote Pacific and TOMS data indicate the presence of absorbing aerosols, it is possible that the major absorbing aerosol is not dust but black carbon but their temporal variability is similar.

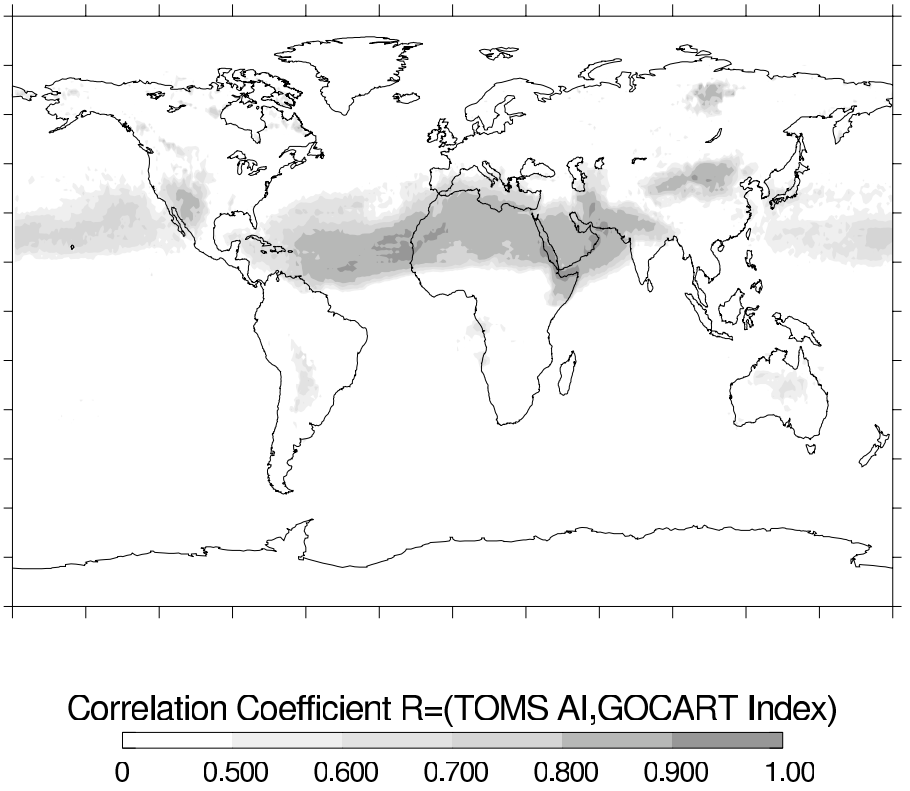

Fig. 7. Global distribution of the correlation coefficient (R) between the TOMS AI and an index calculated with the model results and TOMS viewing angles from January 1981 to December 1990.

6. Effects of North Atlantic Oscillation on dust distribution

In this section, we examine the inter-annual variability of dust distribution in relation to the NAO. The NAO exerts a strong influence on the large-scale variations of both the atmospheric circulation and the hydrological cycle in the Northern hemisphere. Hurrell (1995) defined a NAO index which is calculated by taking the difference between normalized sea-level atmospheric pressures between Lisbon, Portugal, and Stykkisholmur, Iceland. Winters with high NAO indices are characterized by a deepening of the Icelandic low associated with a stronger Azores anticyclone. This yields higher surface pressure and drier conditions over Northern Africa. During low NAO conditions, there is an increase of precipitation over the Mediterranean and North Africa. Moulin et al. (1997) have shown that both pattern and intensity of the transport of African dust are affected by the NAO.

Fig. 8 shows the year-to-year variability of the NAO winter index values from http://www.cgd.ucar.edu/~jhurrell/nao.html, and the simulated and observed dust concentration at Barbados in winter (January–March). There is no data at Barbados from December 1981 to March 1982. The correlation coefficients (R) between the NAO index and the simulated and observed concentrations are 0.67 and 0.5, respectively. For the other seasons, there is no significant correlation. If one uses the corresponding season of the NAO index, the correlation does not improve, mainly because the pressure difference between Iceland and Portugal is much weaker, and thus its effects on the meteorology. On the other hand, the NAO index is mostly positive during our simulation, and longer periods with stronger variation of the NAO index would provide better constrain in summer.

Fig. 9 shows the distribution of the correlation coefficient between the NAO winter index and the winter dust emission, surface concentration and columnar mass, from 1981 to 1996. There is a high correlation (>0.9) with the dust emission from the Bodele depression–Lake Chad region which is the most active African source in winter (cf. Table 4) and the most active dust source on Earth at present (Prospero et al., 2002). The year-to-year variability of surface concentration in winter seems to be correlated with the NAO over much of the North Atlantic and the western part of North Africa. Similar correlation exists for the dust mass column, although to a lesser extent. The NAO modulates the year-to-year variability of dust emission in winter, but it is unclear if the year-to-year variability of surface concentration and mass column is due to the modulation of the emission or transport.

A limitation of our study is due to the relatively short period considered which covers mostly positive values of the NAO index. By considering the 36 years of

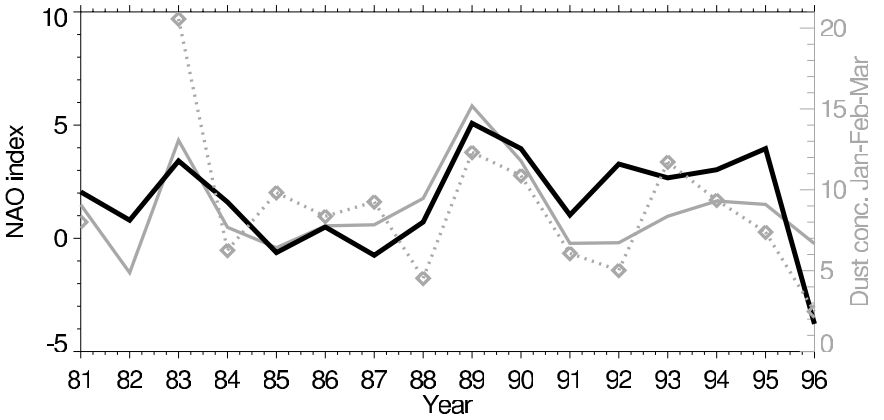

Fig. 8. Comparison between NAO index (bold black line) and the simulated (gray continuous line) and observed (diamonds and gray dashed line) surface concentration in winter at Barbados, from 1981 to 1996, in units of μg m^{-3}.

recorded data at Barbados from 1965, the correlation coefficient with the NAO index is only 0.26. Therefore, it is unlikely that the two are correlated at Barbados. However, it does not mean that the NAO is not controlling dust emission over North Africa, and dust distribution over the Western part of the North Atlantic. Indeed, the dust plumes over the Atlantic are transported generally South of Barbados in winter (Husar et al., 1997). Comparison with satellite data (e.g. TOMS index) could be helpful to determine the spatial extend of the NAO effect on dust distribution over the Atlantic. However, GOCART model indicates that aerosols from biomass burning activity during the dry season in West Africa contribute for most of the aerosol loading in the tropical Atlantic (Chin et al., 2002), and it is difficult to separate aerosol components from satellite data.

7. Conclusions

The dust size distribution in the atmosphere is simulated with the GOCART model from 1981 to 1996. The major features of the dust model are that it is driven by the NASA GEOS DAS assimilated meteorological fields and the dust sources are associated with bare soils in topographic lows. The seasonal and inter-annual variability of surface concentrations have been compared with in situ measurements. The model performs correctly in the dusty regions but tends to damp the seasonal variation in the remote atmosphere: simulated values overestimated in winter and underestimated in summer. A difficulty to correct such discrepancy is that it could come from different processes, including numerical diffusion. This last possibility is clearly apparent when studying a dust event in March 1988. This dust event was analyzed by calculating an index equivalent to the TOMS AI.

The budget over the different continents and oceans has been compared. Globally, the maximum difference of annual emission from 1981 to 1996 is about 23% with the lowest emission in 1996 (1950 Tg) and the highest in 1988 (2400 Tg). The dust removal by wet deposition contributes globally by only 10% but with important regional variations. Over the North Pacific the wet deposition is about 50% of the total loss. The dust deposition over the Indian Ocean (northern hemisphere) is as important, annually, than over the North Atlantic. The annual mean North African emission is about 1400 Tg which corresponds to 65% of the global emission. The second major source region is East Asia which contributes for 25%. Although North America has active dust sources in the south-west, it constitutes a sink for dust by about 30 Tg $year^{-1}$. This result indicates the importance of inter-continental transport. The analysis of the budget over Africa confirms that dust emission shifts from Sahel and Sahara following the seasonality of the ITCZ latitudinal movements. Each region presents a different inter-annual variability.

The inter-annual variability of dust distribution and emission is compared with the NAO index. It is shown that the winter surface concentration is correlated with the NAO index over much of the North Atlantic and western Africa, in relation to a strong correlation of the emission over the Bodele depression–Lake Chad region.

The simulated period covers only two cycles of the NAO with its index mostly positive. Previous decades showed mostly negative values of the index. The 36 years recorded dust concentration at Barbados indicates that there is no correlation between surface concentration in winter and the NAO index. The forthcoming release of 40 years re-analysis by the European Center for Medium range Weather Forecasting (ECMWF) will hopefully provide reliable information needed to understand if the effects of the NAO on dust distribution is rather limited or if Barbados is at the edge of the affected region.

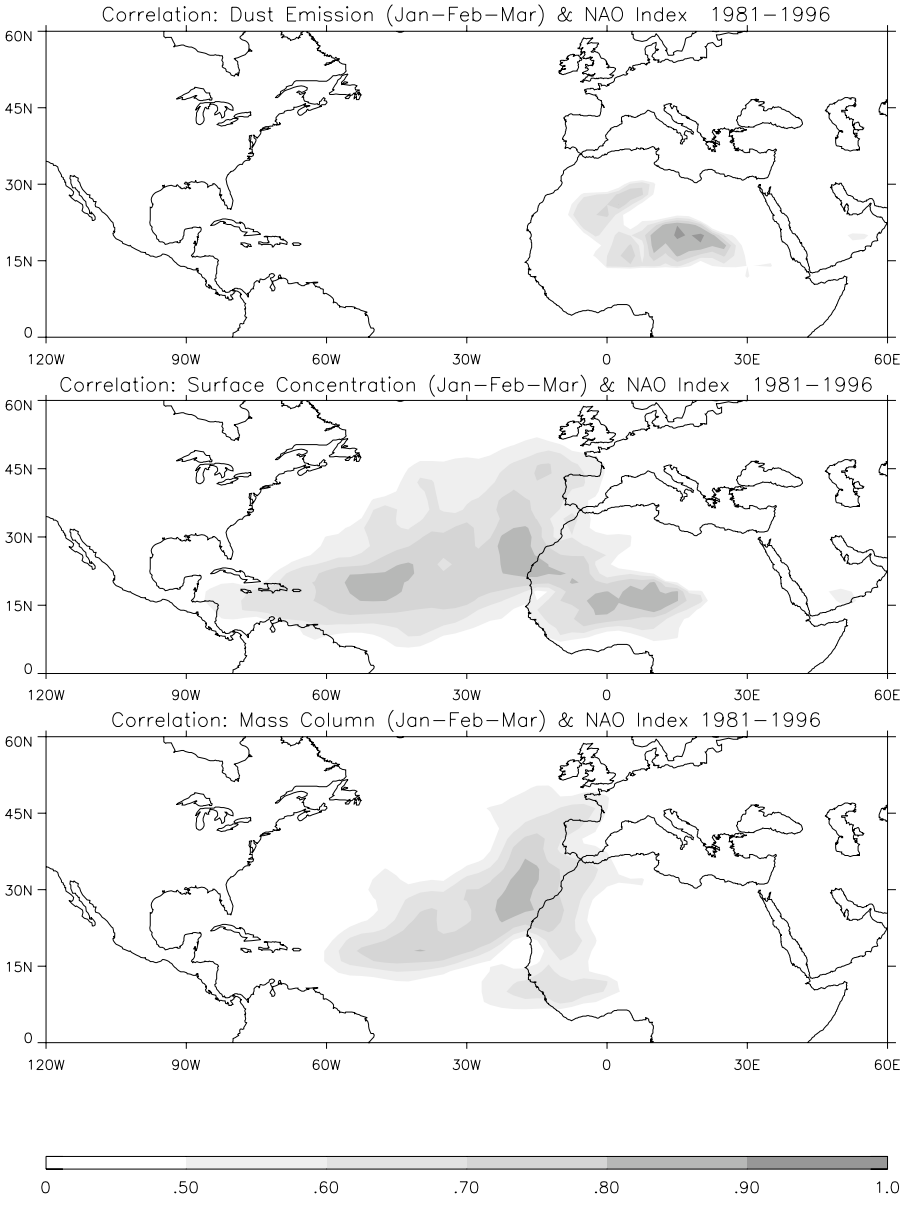

Fig. 9. Global distribution of the correlation coefficient (*R*) between the NAO index and the winter (January–February–March) simulated dust emission (upper panel), surface concentration (middle panel), and mass column (lower panel), from 1981 to 1996.

Acknowledgements

The authors thank the TOMS OPT team for producing the TOMS aerosol data set, Ms. Andrea Molod for her help in using DAO data and Mr. Richard Rood to give us access to these data. This work was supported in part by the NASA grant NAG-35-694, and the NASA Global Aerosol Climate Project (GACP).

References

Alpert, P., Krichak, S.O., Tsidulko, M., Shafir, H., Joseph, J.H., 2002. A dust prediction system with TOMS initialization. Mon. Weather Rev. 130, 2335–2345.

Arimoto, R., Duce, R.A., Ray, B.J., Ellis, W.G. Jr., Cullen, J.D., Merrill, J.T., 1995. Trace elements in the atmosphere over the North Atlantic. J. Geophys. Res. 100, 1199–1213.

Arimoto, R., Snow, J.A., Graustein, W.C., Moody, J.L., Ray, B.J., Duce, R.A., Turekian, K.K., Maring, H.B., 1999. Influences of atmospheric transport pathways on radionuclide activities in aerosol particles from over the North Atlantic. J. Geophys. Res. 104, 21.

Barnum, B., Winstead, N.S., Wesely, J., Hakola, A., Colarco, P.R., Toon, O.B., Ginoux, P., Brooks, G., Hasselbarth, L., Toth, B. Forecasting dust storms using CARMA-dust model and MM5 weather data. J. Environ. Model. Software, this issue, doi: 10.1016/S1364-8152(03)00115-4.

Chiapello, I., Moulin, C., 2002. TOMS and METEOSAT satellite records of the variability of Saharan dust transport over the Atlantic during the last two decades (1979–1997). Geophys. Res. Lett. 29, 1176, doi:10.1029/2001GL013767.

Chin, M., Rood, R.B., Lin, S.-J., Müller, J.-F., Thompson, A., 2000.

Atmospheric sulfur cycle simulated in the global model GOCART: model description and global properties. J. Geophys. Res. 105, 24.

Chin, M., Ginoux, P., Kinne, S., Torres, O., Holben, B., Duncan, B.N., Martin, R.V., Logan, J., Higurashi, A., Nakajima, T., 2002. Tropospheric aerosol optical thickness from the GOCART model and comparisons with satellite and sun photometer measurements. J. Atmos. Phys. 59, 461–483.

Colarco, P.R., Toon, O.B., Torres, O., Rasch, P.J., 2002. Determining the UV imaginary index of refraction of Saharan dust particles from TOMS data and a three dimensional model of dust transport. J. Geophys. Res. 107, 4289, doi: 10.1029/2001JD000903.

Dentener, F.J., Carmichael, G.R., Zhang, Y., Lelieveld, J., Crutzen, P.J., 1996. Role of mineral aerosol as a reactive surface in the global troposphere. J. Geophys. Res. 101, 22.

Dickerson, R.R., Kondragunat, S., Stenchikov, G., Civerolo, K.L., Doddridge, B.G., Holben, B.N., 1997. The impact of aerosols on solar ultraviolet radiation and photochemical smog. Science 278, 827–830.

Dubovik, O., Holben, B., Eck, T.F., Smirnov, A., Kaufman, Y.J., King, M.D., Tanré, D., Slutsker, I., 2002. Variability of absorption and optical properties of key aerosol types observed in worldwide locations. J. Atmos. Sci. 59, 590–608.

Gillette, D.A., Passi, R., 1988. Modeling dust emission caused by wind erosion. J. Geophys. Res. 93, 14.

Ginoux, P., Chin, M., Tegen, I., Prospero, J.M., Holben, B., Dubovik, O., Lin, S.J., 2001. Sources and distributions of dust aerosols simulated with the GOCART model. J. Geophys. Res. 106, 20.

Ginoux, P., Torres, O. Empirical TOMS index for dust aerosol: applications to model validation and source characterization. J. Geophys. Res., in press.

Gregg, W., Ginoux, P., Schopf, P.S., Casey, N.W. Phytoplankton and Iron: validation of a global three-dimensional ocean biogeochemical model. Deep Sea Res., in press.

Herman, J.R., Bhartia, P.K., Torres, O., Hsu, C., Seftor, C., Celarier, E., 1997. Global distribution of UV-absorbing aerosols from Nimbus 7/TOMS data. J. Geophys. Res. 102, 16.

Hurrell, J.W., 1995. Decadal trend in the North Atlantic Oscillation: regional temperatures and precipitations. Science 269, 676–679.

Husar, R.B., Prospero, J.M., Stowe, L.L., 1997. Characterization of tropospheric aerosols over the oceans with the NOAA advanced very high resolution radiometer optical thickness operational product. J. Geophys. Res. 102, 16.

Iversen, J.D., White, B.R., 1982. Saltation threshold on Earth, Mars and Venus. Sedimentology 29, 111–119.

Liao, H., Yung, Y.L., Seinfeld, J.H., 1999. Effects of aerosols on tropospheric photolysis rates in clear and cloudy atmospheres. J. Geophys. Res. 104, 23.

Mahowald, N.M., Zender, C., Luo, C., Savoie, D., Torres, O., del Corral, J., 2002. Understanding the 30-year Barbados desert dust record. J. Geophys. Res. 107, 4561, doi:10.1029/2002JD002097.

Marticorena, B., Bergametti, G., 1995. Modeling the atmospheric dust cycle: 1. Design of a soil-derived dust emission scheme. J. Geophys. Res. 100, 16.

Martin, J.H., Gordon, R.M., 1988. Northeast Pacific iron distributions in relation to phytoplankton productivity. Deep Sea Res. 35, 177–196.

Martin, R.V., Jacob, D.J., Logan, J.A., Bey, I., Yantosca, R.M., Staudt, A.C., Li, Q., Fiore, A.M., Duncan, B.N., Liu, H., Ginoux, P., Thouret, V., 2002. Interpretation of TOMS observations of tropical tropospheric ozone with a global model and in situ observations. J. Geophys. Res. 107 (4351), doi:10.1029/2001JD001480.

Mbourou, N.G., Bertrand, J.J., Nicholson, S.E., 1997. The diurnal and seasonal cycles of wind-borne dust over Africa North of the equator. J. Appl. Meteo. 36, 868–882.

Merrill, J.T., Uematsu, M., Bleck, R., 1989. Meteorological analysis of long range transport of mineral aerosols over the North Pacific. J. Geophys. Res. 94, 8584–8598.

Moulin, C., Lambert, C.E., Dulac, F., Dayan, U., 1997. Control of atmospheric export of dust from North Africa by the North Atlantic Oscillation. Nature 387, 691–694.

Penner, J.E., et al. 2001. Their direct and indirect effects. In: Houghton, J.T. (Ed.), Climatic Change: The Scientific Basis. Cambridge University Press, pp. 289–348.

Penner, J.E., et al. 2002. A comparison of model- and satellite-derived aerosol optical depth and reflectivity. J. Atmos. Phys. 59, 441–460.

Perry, K.D., Cahill, T.A., Eldred, R.A., Dutcher, D.D., Gill, T.E., 1997. Long-range transport of North African dust to the eastern United States. J. Geophsy. Res. 102, 11.

Prospero, J.M., 1999. Long-term measurements of the transport of African mineral dust to the Southeastern United States: implications for regional air quality. J. Geophys. Res. 104, 15.

Prospero, J.M., Blades, E., Mathison, G., Naidu, R. Interhemispheric transport of viable fungi and bacteria from Africa to the Caribbean with soil dust. Global Biogeochem. Cycles, in press.

Prospero, J.M., Ginoux, P., Torres, O., Nicholson, S., Gill, T., 2002. Environmental characterization of global sources of atmospheric soil dust derived from the Nimbus 7 total ozone mapping spectrometer (TOMS) absorbing aerosol product. Rev. Geophys. 40 (1), 1002, doi:10.1029/2000RG000095.

Prospero, J.M., Nees, R.T., 1986. Impact of the North African drought and El Nino on the mineral dust in the Barbados trade winds. Nature 320, 735–738.

Prospero, J.M., Schmitt, R., Cuevas, E., Savoie, D.L., Graustein, W.C., Turekian, K.K., Volz-Thomas, A., Diaz, A., Oltmans, S.J., Levy II, H., 1995. Temporal variability of summer-time ozone and aerosols in the free troposphere over the eastern North Atlantic. Geophys. Res. Lett. 22, 2925–2928.

Savoie, D.L., Prospero, J.M., 1977. Aerosol concentration statistics for the tropical North Atlantic. J. Geosphys. Res. 82, 5954–5963.

Sokolik, I.N., Toon, O.B., 1996. Direct radiative forcing by anthropogenic airborne mineral aerosol. Nature 381, 681–683.

Tegen, I., Lacis, A.A., 1996. Modeling of particle size distribution and its influence on the radiative properties of mineral dust aerosol. J. Geophys. Res. 101, 19.

Torres, O., Bhartia, P.K., Herman, J.R., Ahmad, Z., Gleason, J., 1998. Derivation of aerosol properties from satellite measurements of backscattered ultraviolet radiation: theoretical basis. J. Geophys. Res. 103, 17.

Torres, O., Bhartia, P.K., Herman, J.R., Sinyuk, A., Ginoux, P., Holben, B., 2002. A long-term record of aerosol optical depth from TOMS observations and comparison to AERONET measurements. J. Atmos. Sci. 59, 398–413.

Weaver, C., Ginoux, P., Hsu, N., Chou, M.-D., Joiner, J., 2002. Radiative forcing of Saharan dust: GOCART model simulations compared with ERBE data. J. Atmos. Sci. 59, 736–747.